An Adaptive PV Frequency Control Strategy Based on Real-Time Inertia Estimation

Yu Su, *Student Member, IEEE*, Hongyu Li, *Student Member, IEEE*, Yi Cui, *Member, IEEE*, Shutang You, *Member, IEEE*, Yiwei Ma, *Member, IEEE*, Jingxin Wang, *Member, IEEE*, and Yilu Liu, *Fellow, IEEE*

***Abstract*—The declining cost of solar Photovoltaics (PV) generation is driving its worldwide deployment. As conventional generation with large rotating masses is being replaced by renewable energy such as PV, the power system's inertia will be affected. As a result, the system's frequency may vary more dramatically in the case of a disturbance, and the frequency nadir may be low enough to trigger protection relays such as under-frequency load shedding. The existing frequency-watt function mandated in power inverters cannot provide grid frequency support in a loss-of-generation event, as PV plants usually do not have power reserves. In this article, a novel adaptive PV frequency control strategy is proposed to reserve the minimum power required for grid frequency support. A machine learning model is trained to predict system frequency response under varying system conditions, and an adaptive allocation of PV headroom reserves is made based on the machine learning model as well as real-time system conditions including inertia. Case studies show the proposed control method meets the frequency nadir requirements using minimal power reserves compared to a fixed headroom control approach.**

***Index Terms*—Adaptive control, frequency response, frequency nadir, machine learning, power system inertia, PV, wide-area measurements.**

I. Introduction

RENEWABLE energy plays a critical role in energy security and sustainability. As fossil fuels face depletion, they are being replaced by renewable energy resources worldwide. Solar photovoltaics (PV) has gained a lot of momentum in deployment, driven by enabling inverter technologies, decreasing solar panel costs, as well as decreasing energy storage system costs.

The United States has substantial solar resources [1]. The Sunshot Initiative of the U.S. Department of Energy envisions that solar PV will generate 14% of the total electrical energy in the U.S. by 2030, and by 2050, solar PV will generate 27% of the total electricity in the U.S. [2].

Driven by the continuing trend in solar PV deployment, researchers have been studying the impact of increasing renewable generation on power system stability, especially inverter-based sources such as solar PV and some wind turbines. Without proper control, the inverter-based sources would be simply replacing conventional generators with turbine governors and rotating masses, which would adversely affect the system's frequency response. Some preliminary studies in the U.S. power grids demonstrated that overall frequency response would deteriorate significantly with increased renewable penetration [3]–[5]. Similar studies showed that insufficient inertia would negatively influence the frequency regulation in South Australia power grid with high penetration of renewable generation [6]. In [7], the Irish power grid faces challenges in operating at 50% penetration of wind generation because of reduced inertia. Simulation studies in the U.S. WECC system [8] reveal vulnerabilities brought by extremely high wind penetrations and explores potential mitigating approaches.

After reviewing system studies on several power grids with increasing PV and wind penetrations, the North American Electric Reliability Corporation (NERC) has determined that additional control strategies and resources are required to meet the primary frequency control demand as renewable penetration increases [9]. As a result, the frequency-watt function [10], which is analogous to the governors in conventional generators, has become a standard requirement in North American power grids. Moreover, studies show that synthetic inertia control of inverters that emulate the inertia response of synchronous generators help regulate the system's frequency response [11]–[17].

The majority of PV inverters online operate in grid-following mode, where the inverter regulates the output current magnitude and angle [18]. The other control mode is the grid-forming mode, where the inverters control the output voltage and frequency. While wind-turbines typically have the ability to reserve power for frequency response [19], the inverters are

Manuscript received March 9, 2020; revised August 28, 2020; accepted December 13, 2020. Date of publication December 17, 2020; date of current version April 21, 2021. This work was supported in part by the U.S. Department of Energy under Award 34231; in part by the Department of Energy through NSF Award under Grant EEC-1041877; and in part by the CURENT Industry Partnership Program. Paper no. TSG-00337-2020. *(Corresponding author: Yu Su.)*

Yu Su, Hongyu Li, Shutang You, Yiwei Ma, and Jingxin Wang are with the Department of Electrical Engineering and Computer Science, University of Tennessee, Knoxville, TN 37996 USA (e-mail: ysu10@utk.edu; hli90@utk.edu; syou3@utk.edu; yma13@utk.edu; jwang78@utk.edu).

Yi Cui is with the School of Information Technology and Electrical Engineering, University of Queensland, Brisbane, QLD 4072, Australia (e-mail: y.cui3@uq.edu.au).

Yilu Liu is with the Department of Electrical Engineering and Computer Science, University of Tennessee, Knoxville, TN 37996 USA, and also with the Power and Energy Systems Group, Oak Ridge National Laboratory, Oak Ridge, TN 37830 USA (e-mail: liu@utk.edu).

Color versions of one or more figures in this article are available at https://doi.org/10.1109/TSG.2020.3045626.

Digital Object Identifier 10.1109/TSG.2020.3045626

controlled to output the maximum available power based on Maximum Power Point Tracking (MPPT) to take advantage of the low marginal cost of PV generation versus conventional generation, such as gas or coal. However, as the penetration of renewables such as PV increases, there may not be enough primary frequency response resources in an under-frequency event such as loss of generation, if there is no real power reserve available in the PV inverters. While the power reserve control strategy is readily available at the inverter level [20], and frequency-watt curve has been studied at the system level [10], there is a research gap in the determination and scheduling of PV real power reserves. Although other grid resources, such as energy storage systems and supercapacitors can be utilized to improve primary frequency response [21]–[23], they require additional planning, design, and investment. If there is insufficient real power reserve, especially in high renewable penetration scenarios, the system risks lower frequency nadirs in severe contingencies, which may cause under-frequency tripping of loads and/or inverters. On the other hand, PV real power reserve means lost generation with low marginal costs. Therefore, there is great importance and economic value from the system's frequency response standpoint in developing a model that dispatches the PV real power reserves according to system requirements and conditions.

The main contributions of this article are twofold: we reduce the error of inertia estimation using ambient PMU measurements from 12% (the state-of-the-art method in the literature) to 5%; based on the real-time system inertia estimation, we propose a novel PV real power reserve dispatch model leveraging real-time system inertia estimation and conventional generation dispatch signals. The goal of the dispatch is to meet system frequency response requirements utilizing minimal PV power reserve. A machine learning model is trained using time-domain simulation data from a realistic power system model, and used to predict the frequency nadir of a predetermined contingency, given the estimation of system inertia and dispatch of conventional generators. For each set of system conditions (system inertia, available non-PV generation participating in primary frequency response), a one to one correlation between system PV real power reserve and frequency response nadir of the predetermined contingency can be established using the machine learning model. The minimal PV power reserve that keeps the frequency nadir above the predefined threshold is selected as the optimal dispatch. Studies on a test system based on the U.S. Electric Reliability Council of Texas (ERCOT) system shows that the PV real power reserve dispatch maintains the system frequency response nadir above the pre-determined threshold in the resource contingency criteria (RCC). The dispatch also generates a 50% savings in PV real power reserve compared to a dispatch that fixes the PV real power reserve throughout the day. We also show that the control method performs well using noisy measurements on a power electronics converter-based grid emulator.

The remainder of this article is organized as follows. The design and implementation of our real-time inertia estimation algorithm is introduced in Section II. The adaptive PV frequency control is proposed and explained in detail in Section III. Section IV shows the validation case study on a realistic large power system simulation model. The control method is tested in a hardware-in-the-loop test platform in Section V. The conclusions are given in Section VI.

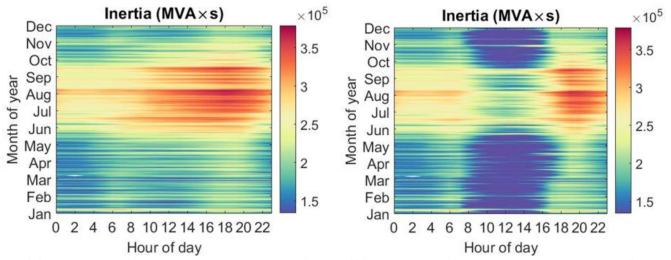

(a) 10% peak PV power penetration (b) 50% peak PV power penetration

Fig. 1. Inertia variations in different levels of PV penetration.[1]

II. System Inertia Variation and Real-Time Estimation

Power system inertia consists mostly of the rotating inertia in synchronous generators, some motor loads, and potentially future renewable power plants if they provide synthetic inertia, and can vary throughout the day. Fig. 1 shows the projected daily and yearly inertia variations of the ERCOT system at the current and future PV penetration scenarios. The PV penetration is defined as the percentage of PV's output power in the system's total load. With more PV generation during the day, synchronous generators are displaced, and the system inertia will drop, as indicated in Fig. 1 (b). The gap between peak and bottom inertia grows larger as PV penetration climbs higher.

Wide-area measurement systems provide time-synchronized grid measurements that can be used to estimate system inertia [24]–[28]. Although power system inertia estimation has been heavily investigated in the literature, most use frequency disturbance data, which suggests that inertia was calculated offline. In this article, we use ambient frequency measurements to estimate the system inertia in real-time, and increase the state-of-the-art accuracy of inertia estimation using ambient synchrophasor frequency measurements from 12% mean absolute percentage error [28] to less than 5%. The estimation of inertia is at the system level, which is the sum of the inertia of the generators (and motor loads) in the system. This provides a solid basis for the proposed adaptive PV frequency control.

A. Multivariate Random Forest Regression (MRFR)

In this study, we use the available inertia data, load profile, extracted features in the ambient frequency measurements at different locations, and weather data (average ambient temperature) to train a multivariate regression model for system inertia estimation. For application with very large amounts of training data, we use Multivariate Random Forest Regression (MRFR) as the machine learning model to estimate

[1] Available online: https://www.energy.gov/sites/prod/files/2019/08/f65/3.2.d.%20-%20SETO%20Modeling%20Workshop%20-%20ORNL.pdf.

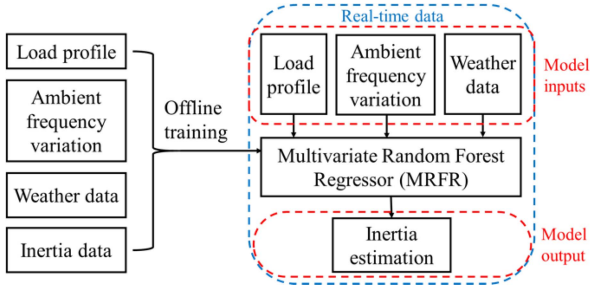

Fig. 2. Data flow of the inertia estimation algorithm.

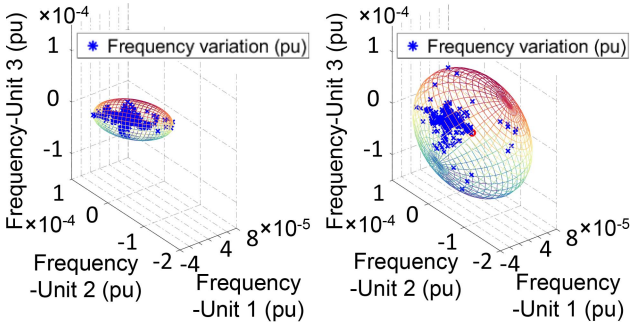

(a) 100% inertia level (b) 50% inertia level

Fig. 3. Minimum volume enclosing ellipsoids at different inertia levels.

the system inertia. MRFR is an ensemble of regression trees trained by bootstrap sampling and random feature selection. Due to the length restrictions of this article, interested readers are referred to [29].

It is worth noting that other machine learning algorithms such as neural nets and support vector machines are also applicable to this inertia estimation method. We chose MRFR in this study due to its high robustness to the input data, its capability to avoid overfitting the training data, and its overall best performance in terms of estimation accuracy.

We can sum up the data flow of the online inertia estimation algorithm, which is shown Fig. 2. Before application, the MRFR is trained using available offline data. In real-time application, the trained MRFR will receive online measurements and extracted features, and use them to estimate the total inertia of the power system. While the inertia data, load profile, and weather data are readily available from reliability coordinators and transmission operators, the features from ambient frequency measurements need to be extracted from the raw frequency data. It is worth mentioning that by using the ambient frequency measurement, we are able to account for virtual inertia emulated by inverter-interfaced renewable resources, since its effects on ambient frequency variations can be captured and converted to equivalent inertia. In the next section, we will discuss the method to extract features from ambient frequency data.

B. Ambient Frequency Data Feature Extraction

The raw frequency time-series data from multiple PMUs in the power system is piped through a data pre-processing process, which includes data continuity check, outlier detection, and temporal alignment. We use the processed data to extract the frequency variations of the frequency time-series data measured from multiple PMUs across the power grid, defined as the frequency deviation from the mean of the frequency measurements.

Once the variation of the ambient frequency data from each PMU is calculated, we use a series of time windows with fixed width to divide the time series data and use the Minimum Volume Enclosing Ellipsoid (MVEE) [30]–[32] method to construct the characteristic ellipsoids and extract the informative features from each data segment for inertia estimation. MVEE provides a novel method to monitor system status and estimate its dynamic behaviors by interpreting the graphic parameters of a multi-dimensional closed ellipsoid. Such ellipsoid with minimum volume is calculated by enclosing a certain part of the system frequency trajectory in the phasor measurement space. We use the frequency measurement matrix $\boldsymbol{\theta_M}$, defined as:

$$\boldsymbol{\theta_M} = \begin{bmatrix} \theta_{11} & \cdots & \theta_{1m} \\ \vdots & \ddots & \vdots \\ \theta_{n1} & \cdots & \theta_{nm} \end{bmatrix}, \; n < m \tag{1}$$

where n is the number of PMUs, m is the length of the time window imposed on the frequency measurements. An ellipsoid (*hyper-ellipsoid*) that contains the measurements can be expressed as:

$$H_{A,C} = \left\{ \theta \in \Omega^{\,n} \middle| (\theta - c)^T A (\theta - c) \leq 1 \right\} \tag{2}$$

where A is a positive definite matrix and θ, c are vectors of n dimensions in the phasor measurement space. The volume of the ellipsoid is expressed as

$$Vol(H_{A,C}) = \pi^{\frac{n}{2}} \Big/ \Gamma\left(\frac{n+2}{2}\right) \sqrt{\det\ (A))} \tag{3}$$

where Γ is the gamma function:

$$\Gamma(n/2) = (n-2)!!\sqrt{n/2^{(n-1)/2}} \tag{4}$$

$$n!! = \begin{cases} n \times (n-2) \times \cdots \times 3 \times 1, & n > 0, \; odd \\ n \times (n-2) \times \cdots \times 4 \times 2, & n > 0, \; even \\ 1, & n = -1, 0 \end{cases} \tag{5}$$

We obtain the ellipsoid with minimum volume by minimizing $-\ln(\det A)$, using interior-point methods.

The correlation between the parameters of the MVEE and the trajectory of the system frequency measurements lies in the volume and shape of the MVEE. We use simulated ambient data from a power system model of the U.S. Eastern Interconnection with randomly varying loads under two inertia levels – 100% and 50%. The inertia levels here are the relative system inertia values, with 100% being the baseline. It should be noted that the applied load variation is very small compared to the base load. Two ellipsoids can be constructed from 60-second frequency data. Due to the difficulties of representing hyper-ellipsoids graphically, we used frequency measurements from only three units. The ellipsoids are shown in Fig. 3. The ellipsoids are constructed in the frequency space, and the numbers in the figure are per unit values. We can observe significant differences in the graphical parameters of the ellipsoids.

Based on the above analyses, we can use the graphical parameters of the MVEE, including volume, center vectors, projections of the longest semi-axis along each dimension, and the eccentricity as descriptive features to estimate the system inertia. Based on the reporting rate of the available system inertia data used for training, we divide the ambient frequency measurements into the number of segments equal to the number of inertia data points. In our case, we have inertia data reported at 10-minute intervals. This means we have 144 segments in one day. For each of the 144 frequency segments, we use a 5-minute sliding window with a 10-second step to step through the segments and calculate the characteristic ellipsoids. For each segment the descriptive features from the characteristic ellipsoids are averaged and used as inputs to the MRFR. More description on the inertia estimation method can be found in [40].

C. Performance Evaluation

To evaluate the performance of the MRFR based real-time inertia estimation algorithm, we use a testing dataset that's independent from the training dataset. The testing dataset spans a whole year and includes system inertia data, synchrophasor measurements of the U.S. WECC system from GridEye [35], actual weather data (average ambient temperature of six cities in WECC system, including Los Angeles, Phoenix, Salt Lake City, Denver, Las Vegas, and Seattle), and system generation and load data. We used measurements from 20 Frequency Disturbance Recorders (FDRs) [35] deployed in the WECC system. More details on their geographical distribution can be found online.[2]

During the training process, we used a 5-minute time window and a 10-second step size. Since the reporting interval of the inertia data is 10 minutes, 30 sets of MVEEs are generated for each 10-minute interval and each measurement. The graphical features of the MVEEs are averaged within the same 10-minute window and used to train the MRFR.

The metrics used for performance evaluation are absolute percentage error (APE) and mean absolute percentage error (MAPE), defined as:

$$APE_i = \left| \frac{M_i^{'} - M_i}{M_i} \right| \times 100\% \tag{6}$$

$$MAPE = \frac{1}{m} \sum_{i=1}^{m} APE_i \tag{7}$$

where $M_i^{'}$ and M_i denote the i-th estimated and measured inertia, respectively, and m is the total number of points estimated.

An example of inertia estimation result is given in Fig. 4. The MAPE for the heavy load season day is 1.2%, and the MAPE for the light load season day is 0.8%. We performed daily inertia estimations for a whole year and evaluated the APE of each estimation point (Fig. 5). The maximum APE of the whole year is 8.7%, and the mean is 3.1%. (It is also found that the estimation errors are on similar levels as load changes and the MAPE does not show significant correlation with the load levels.) Compared to the estimation performance of 12% MAPE in [28], we have reduced the errors dramatically. It is worth mentioning that although the present work and [28] use different test systems, both studies used actual system data in testing.

[2]Available online: http://fnetpublic.utk.edu/.

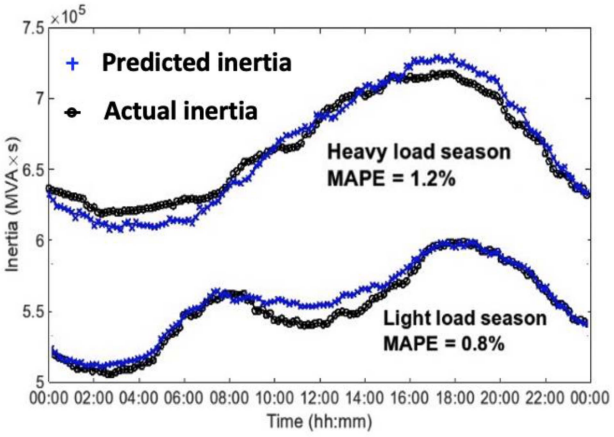

Fig. 4. Estimated and measured inertia in WECC during heavy and light load seasons.

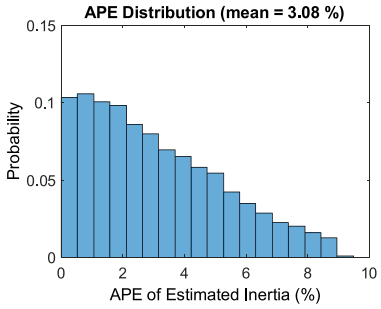

Fig. 5. Inertia estimation error distribution over one year.

In this section, we discussed the system inertia estimation using labeled data. In the case inertia information is not available or inaccurate (for example, uncertainties in load inertia and virtual inertia emulation), we can first classify the system's operation status using the characteristics from the ambient frequency measurements. Then frequency event (generation drop, load trip, etc.) can be utilized to benchmark the system inertia level. As frequency events only happen occasionally in the system, the machine learning-based inertia estimation will require longer time to gather enough measurements to include sufficient frequency event data.

The accuracies of the PMUs that are used to measure the ambient frequency will be affected by the grid transients. However, since our proposed method is based on ambient frequency measurement, which usually does not have any major events or phase jumps, the impacts should be minimal. In addition, the work proposed in [41] developed a frequency measurement technology that is immune to phase jumps in grid transient conditions, which could be used to further mitigate its impact.

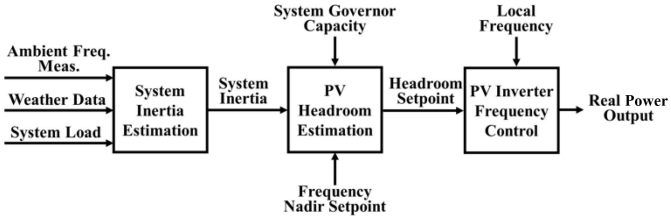

Fig. 6. PV frequency control based on real-time inertia estimation.

III. Adaptive PV Frequency Control Based on Real-Time System Inertia Estimation

A. Control Architecture

Several system conditions, including system inertia and system governor capacity affect the system's frequency response. It is well-established that the relation between various system conditions and frequency nadir is nonlinear. The system conditions also vary throughout the day, especially in future high renewable penetration scenarios. To handle the variabilities in the system conditions and the nonlinearity of the control system, we propose an adaptive PV frequency control method, shown in Fig. 6. There are four steps in this control.

1) Wide-area synchrophasor data and weather information are used for system inertia estimation.
2) System conditions including system inertia and governor capacity are used to estimate the PV headroom requirements.
3) The PV headroom requirements are distributed to the PV plants through communication.
4) PV plants execute headroom setpoints to ensure adequate system frequency response. If a PV plant cannot meet the headroom requirement, the difference will be compensated by other PV plants.

We propose using two machine learning models back-to-back to achieve the adaptive PV frequency control instead of using the end-to-end model that maps the frequency measurements directly to the PV headroom requirement. Although doing so will introduce additional uncertainty to the model, the uncertainty can be regulated by increasing the training dataset. On the other hand, the benefit of this setup is that it can provide the system inertia information as an extra output. The system inertia itself is a very important system metric to ensure system stability and can be utilized by the system operator.

According to the NERC requirements, the PV plants should already have the frequency-watt function, and are monitoring the local frequency. The adaptive controller can be implemented on top of the existing controller with some modifications. The assigned headroom setpoint is transmitted to the local PV plant via Inter-Control Center Communications Protocol (ICCP). Then the PV inverter will regulate its output power based on the headroom setpoint through a power reserve control strategy. An example of such control is presented in [20]. The distribution of PV headroom to multiple PV plants can be integrated into the security-constrained economic dispatch (SCED). For simplicity, we assumed that the headroom is distributed to multiple PV plants according to a fixed percentage (of their real-time dispatch).

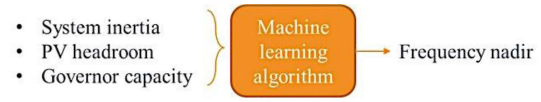

Fig. 7. Inputs and output of the machine learning model.

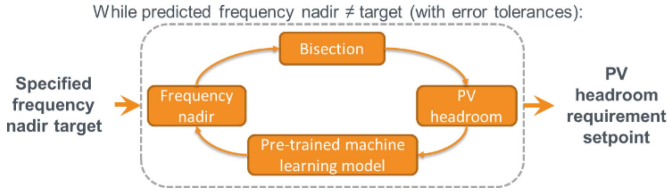

Fig. 8. Real-time PV headroom requirement estimation.

The main control target is the frequency nadir during a pre-determined large contingency, such as the RCC in ERCOT. This criterion gives operators relatively sufficient resources to respond to an emergency without being overly conservative and inefficient. The control is designed to run continuously with headroom setpoints updated periodically based on real-time system conditions.

B. PV Headroom Estimation Model

One crucial process in the adaptive PV frequency control is to have an accurate estimate of the required PV headroom given the system inertia, governor capacity, and frequency response target. Since the relationship between system conditions and frequency response nadir is nonlinear, machine learning methods such as neural networks and random forests can be used to accurately model the relationship between system inertia, system governor capacity, PV frequency control headroom, and system frequency nadir. Fig. 7 shows the inputs and output of the machine learning model. It should be noted that in a realistic large system, there are multiple types of governors for different synchronous generators with different control parameters such as droop and time delay. A clustering step on the different governors helps reduce the dimension of the inputs.

For a given system, the machine learning model can be trained using simulation data or historical data. The trained machine learning model is an adaptive model that predicts the frequency nadir of the RCC. Using the pre-trained model, system inertia, and system governor capacity information, the PV headroom requirement can be estimated for a given frequency nadir target using the bisection method, as shown in Fig. 8.

C. PV Headroom Distribution

After the PV headroom requirement is estimated, it is distributed among the PV plants based on their forecast MPPT power. Currently, the power reserve market for PV generation has not yet been established [33]. Therefore, the distribution of the PV headroom can be as simple as each PV plant contributing the same percentage of PV headroom. Conversely, the PV headroom distribution can be integrated into the security-constrained economic dispatch model where the PV headroom requirement is a constraint on the PV generation dispatch. Due

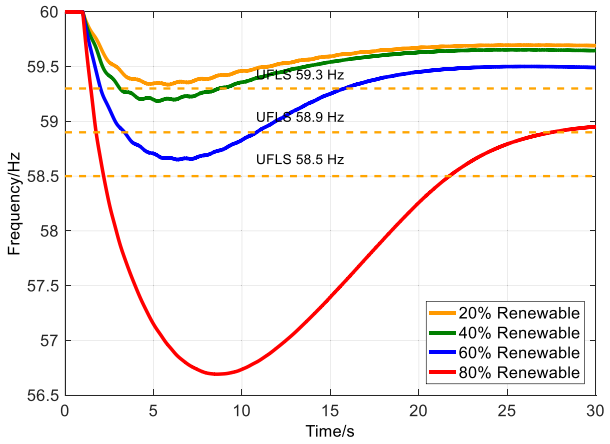

Fig. 9. Frequency response of the ERCOT system under different renewable penetrations.

to the study scope limitation, the method that distributes headroom reserve according to a certain percentage is applied in this study.

IV. Simulation Case Study

A. Simulation System Overview

To evaluate the performance of the proposed adaptive PV frequency control, a series of dynamic simulation is performed on a 6,102-bus power system representing the ERCOT system. The test system is a power system with extra-high instantaneous PV power penetration capabilities, developed and validated in [34]. The frequency response of the ERCOT test system has been validated using both synchrophasor measurements from FNET/GridEye [35] and information of actual events provided by utilities. The model can be adjusted to represent different renewable penetration levels by displacing traditional synchronous generators and/or reducing the system inertia. Fig. 9 shows the frequency response of the test system under different renewable penetrations. When creating the training cases, the effect of varying renewable penetrations is approximated by varying system inertia as well as changing the amount of system turbine governor resources.

The PV frequency control is implemented in the model with the control gain set to 40. The PV headroom is also a parameter that can be modified in the simulation model.

B. PV Headroom Estimation Model

More than 13,000 training cases are created by varying the amount of responsive generation capacity, system inertia, and PV headroom. In each simulation case, the RCC, which is a tripping of 2,750 MW generation in the South Texas Project Nuclear Plant, is simulated, and the frequency response of the system is recorded. A dataset containing governor capacity, system inertia, and PV headroom as inputs and frequency nadir as output is extracted from the simulation cases. A vanilla feedforward neural network is selected as the machine learning algorithm for this study. While other machine learning algorithms are available, the neural network is selected for its wide array of applications backed by a mature theoretical background. Namely, the Universal Approximation Theorem [36] states that a feedforward multilayer neural network is capable of approximating any continuous function, and provides a solid theoretical ground for applying the bisection method. Another consideration when choosing neural networks over other machine learning methods is its ease of tuning and better performance in the training set. Interested readers are referred to [37] for more information on neural networks and its training using backpropagation.

After tuning the hyper-parameters such as the number of the hidden neurons, the number of hidden layers, activation function, we can achieve very high prediction accuracies. The errors on the testing set are in the order of 1 mHz, indicating good performance.

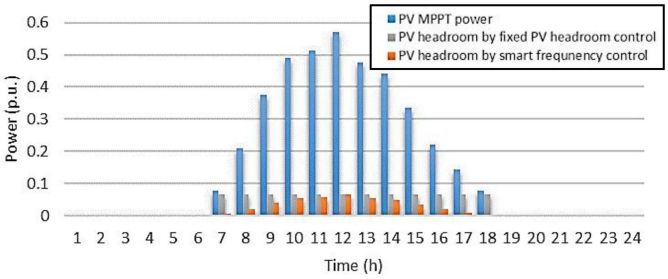

Fig. 10. PV headroom requirement using adaptive PV frequency control and fixed headroom control.

C. Adaptive PV Frequency Control Performance

After the machine learning model is trained, a realistic one-day scenario in ERCOT is created to evaluate the performance of the adaptive PV frequency control. The frequency nadir target is set to 59.5 Hz, which is 0.2 Hz above the Under-Frequency Load Shedding threshold specified by ERCOT. The PV headroom required by the adaptive PV frequency control algorithm is shown in Fig. 10. For reference, a more conservative control strategy where the PV reserves a fixed amount of power for primary frequency response is also shown in Fig. 10.

The control effect of the adaptive PV frequency control is tested against cases with no upward frequency-watt function (no PV headroom), as well as fixed PV headroom. Fig. 11 shows the system average frequency response of the system at different times in the day under different PV frequency control strategies. The plots clearly show that without an upward frequency-watt function, the system cannot keep the frequency nadir above the 59.5 Hz threshold due to decreased system inertia as well as the traditional generation with governors. If a conservative PV reserve amount is kept throughout the day for primary frequency response, some PV generation is forfeit unnecessarily. The proposed adaptive PV frequency control maintains the system frequency nadir above 59.5 Hz while minimizing the PV real power reserve required to do so. A comparison between the adaptive headroom setting and fixed headroom setting shows 48% daily headroom saving.

V. Hardware-in-the-Loop (HIL) Case Study

A. Introduction to CURENT Hardware Testbed (HTB)

The HIL test platform used to test the adaptive PV frequency control is the CURENT HTB, which is built with modular

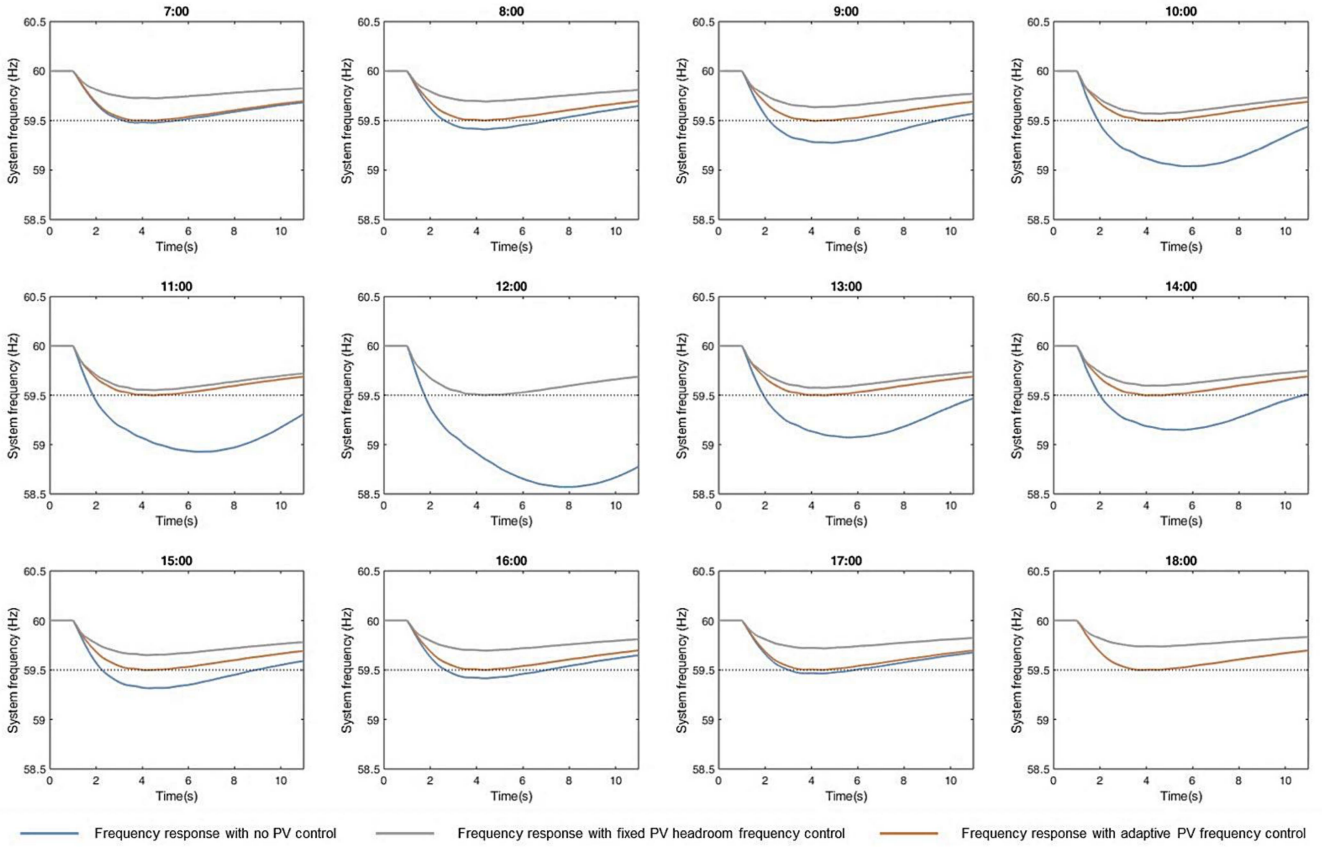

Fig. 11. Frequency response curves of the study day with different PV frequency control strategies.

Fig. 12. CURENT Hardware Testbed (HTB).

and programmable power converters to emulate actual power systems [39]. The HTB is shown in Fig. 12.

In Section IV, the adaptive PV frequency control method has already been tested on a large-scale system. The main goal of the HIL test is to validate the control algorithm in a close-to-real system with measurement noises. To that end, a simple two-area system is set up on HTB, shown in Fig. 13. The test system includes two 200 MW synchronous generators (G1 and G2), one 400 MW PV plant (PV1), and one 365 MW load (L1). Due to the small scale of the test system, tripping either G1 or G2 is likely to cause stability problems in the system. Therefore, we emulate a load step of 80 MW on L1 to mimic a generation drop contingency.

One benefit of testing in a semi-physical testbed like the CURENT HTB is the noisiness of the signals. Although the

Fig. 13. Test system in HTB.

system is in steady state, the frequency measurements still contain background noises. The noise level is measured to be around 5 mHz, which is similar to field measurements from the FNET/GridEye system (Fig. 14). The low-pass filter designed in the adaptive PV frequency control is to filter out such high-frequency noises. A small time constant corresponds to a high cut-off frequency, and reduces the low-pass filter's ability to filter high-frequency noises. On the other hand, a large time constant will also filter out actual frequency transients and delay PV's response to contingencies. Considering the impacts of the time constant, the parameter is set to 0.15. Prior to any implementation in actual systems, the measurement noise needs to be characterized. The time constant is then set accordingly. The control gain of the PV frequency control also impacts system frequency response. A small control gain limits the PV plant's ability to use its power reserves for primary frequency response. On the other hand, if the control gain is too large, the control will be too susceptible to noise and become unstable. In this test, the control gain is set to 100 to maximize power reserve utilization without compromising the stability of the control.

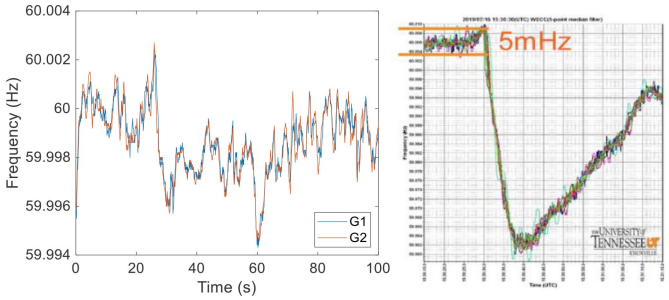

Fig. 14. Ambient frequency measurements in HTB (left) and FNET/GridEye (right).

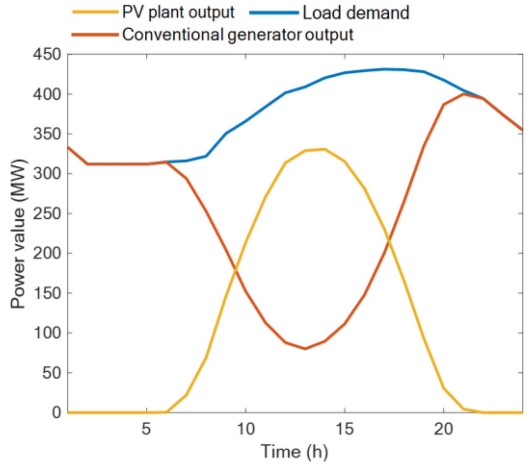

(a) Summer day scenario

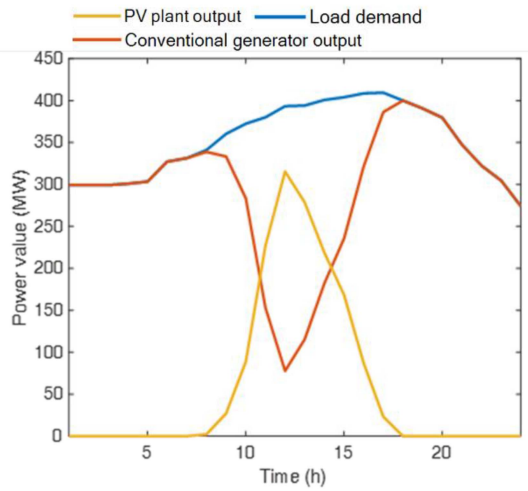

(b) Winter day scenario

Fig. 15. Test scenarios adopted from WECC system data.

B. PV Headroom Estimation Model

Similar to the case study in Section IV, training cases are created by varying system inertia, governor response strength (determined by the governor control gain), and PV headroom. Each training case is created by changing the system setup and emulating the load step increase contingency. 50 frequency response tests are performed on HTB.

A feed-forward neural network with one hidden layer and 70 hidden neurons is trained using the data obtained from the frequency response tests. We use 5-fold cross-validation to validate the trained model. During each round, the training set contains 40 data points, and the testing set contains the remaining 10 data points. The model is able to consistently generate accurate estimates with errors less than 10 mHz.

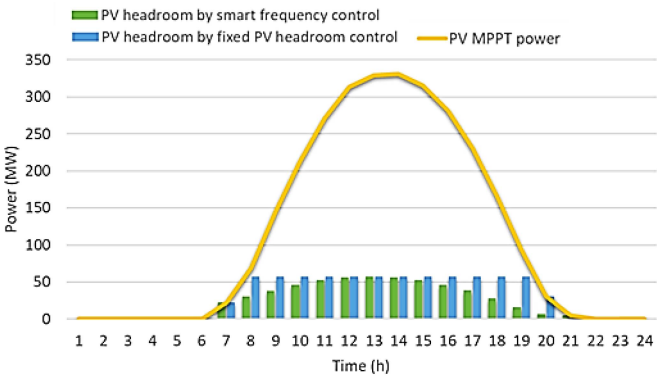

(a) Summer day scenario

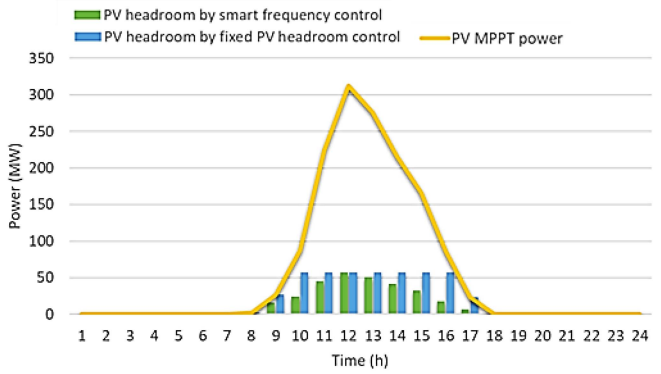

(b) Winter day scenario

Fig. 16. PV headroom determined by adaptive PV frequency control and fixed headroom control.

C. Adaptive PV Frequency Control Performance

To test the performance of the adaptive PV frequency control, two study scenarios consisting of hourly load and PV output profiles in the WECC system are created. The base values for load and PV output are scaled according to the test system setup. The hourly profiles in a future (high penetration of PV) summer day and winter day are shown in Fig. 15. Cloud movement and its impact on PV generation are not considered, since the PV profile is an aggregated profile over a large geographical spread.

In actual large power systems, the system inertia is positively correlated with the total output of online conventional generators. To imitate the actual inertia variations, the inertia value of each generator is scaled according to the dispatch of the conventional generators' output.

We set the frequency nadir target to 59.8 Hz in this experiment. The PV headroom reserve plan is calculated and shown by green bars in Fig. 16, along with the PV headroom reserve plan based on the maximum PV headroom reserve required (blue bars). Compared to the fixed PV headroom reserves, the adaptive PV headroom reserve saves 26% on the summer day and 34% on the winter day.

The adaptive PV frequency control also keeps the frequency nadir around the target, whereas the frequency nadir will drop below target without any control. A comparison of the

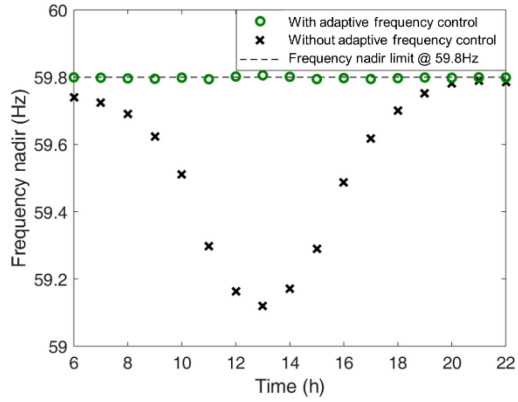

(a) Summer day

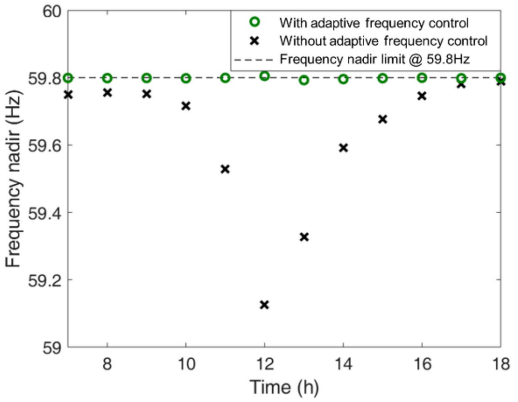

(b) Winter day

Fig. 17. Frequency nadirs of the test system with and without adaptive frequency control.

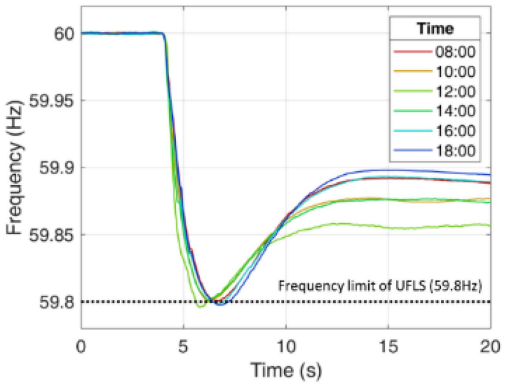

(a) Summer day

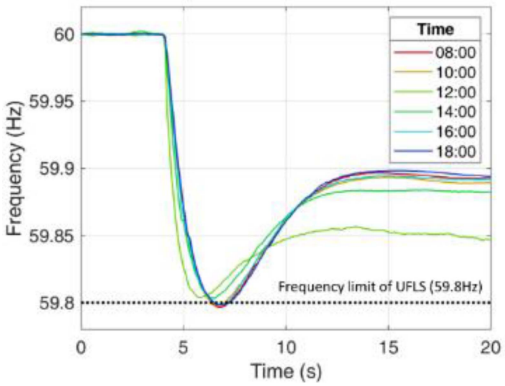

(b) Winter day

Fig. 18. System frequency response at different times with adaptive PV frequency control.

frequency nadirs with and without the adaptive PV frequency control is given in Fig. 17. Since the fixed approach reserves the maximum amount of available PV headroom, it can also meet the frequency nadir target, However, doing so means reserving more PV headroom and economic loss. It should be noted that due to frequency nadir estimation errors, the actual frequency nadir may go below the target. In practice, the frequency nadir target should be higher than the UFLS threshold to avoid accidental load shedding.

It is also observed that the settling frequency (without AGC) during high PV output periods (noon to 2 pm) is lower than that during low PV output periods (early morning, late afternoon), as shown in Fig. 18. This is because the amount of PV power reserve is smaller than the amount of conventional generation reserve to achieve the same frequency nadir. It indicates that PV is more effective in primary frequency control than the conventional generation because of the faster response speed.

VI. Conclusion

A novel adaptive PV frequency control method is presented in this article. The adaptive PV frequency control is necessary for grid frequency support as the power system moves towards higher PV penetration levels.

Through study cases on a realistic large power system, we show that the adaptive PV frequency control method is effective against changing system parameters and can maintain the system frequency nadir above a certain threshold. The simulation results also indicate that in high PV penetration scenarios, the upward frequency-watt function, which is not currently required, may be needed for primary frequency response if primary frequency responsive resources are insufficient. The adaptive frequency control method also saved daily system PV headroom requirement by 48% compared to a conservative fixed PV headroom strategy.

The adaptive PV frequency control method is also tested on a power electronics converter-based grid emulator. We show that by tuning the control gain and low-pass filter, the adaptive PV frequency control method can handle measurement noises in actual grid environments well, while providing sufficient frequency response to limit the frequency nadir above the frequency nadir target. In the HIL test, the adaptive PV frequency control method is able to save on average 30% in PV headroom reserves compared with a fixed PV headroom based on the maximum PV headroom required.

In the future scenario where PV plants are required to provide frequency support to the grid, plant owners can minimize the PV curtailment amount by using the adaptive PV frequency control method. It is worth mentioning that the adaptive approach presents additional cost and complexity in the training and controller implementation. However, the complexity is limited due to the wide availability of machine learning toolboxes including open-source packages in a variety of platforms, the fast computational speed, and existing SCADA communication networks, as well as the wide access of training data provided by grid operators. In conclusion, the economic benefits should be more than enough to offset

the additional cost and complexity brought by the adaptive frequency controller.

In future high renewable penetration scenarios, the proposed adaptive PV frequency control method should work in conjunction with other frequency responsive resources, such as conventional generators, battery energy storage systems, wind turbines, etc. The proposed control method provides a basis for coordinating different frequency responsive resources in future work.

ACKNOWLEDGMENT

The authors gratefully acknowledge the contributions of J. Tan and H. Yuan with the National Renewable Energy Laboratory, and M. Gong with GE Global Research. This work also made use of Engineering Research Center shared facilities supported by the Engineering Research Center Program of the National Science Foundation.

REFERENCES

[1] "Impact of IEEE 1547 standard on smart inverters," IEEE Power Energy Soc., Piscataway, NJ, USA, Rep. PES TR0067, May 2018. [Online]. Available: https://resourcecenter.ieee-pes.org/technical-publications/technical-reports/PES_TR0067_5-18.html

[2] *Sunshot Vision Study*. U.S. Dept. Energy, Washington, DC, USA, Feb. 2012.

[3] H. Pulgar-Painemal, Y. Wang, and H. Silva-Saravia, "On inertia distribution, inter-area oscillations and location of electronically-interfaced resources," *IEEE Trans. Power Syst.*, vol. 33, no. 1, pp. 995–1003, Jan. 2018.

[4] J. Alipoor, Y. Miura, and T. Ise, "Power system stabilization using virtual synchronous generator with alternating moment of inertia," *IEEE J. Emerg. Sel. Topics Power Electron.*, vol. 3, no. 2, pp. 451–458, Jun. 2015.

[5] S. You *et al.*, "Impact of high PV penetration on U.S. eastern interconnection frequency response," in *Proc. IEEE Power Energy Soc. Gen. Meeting*, Chicago, IL, USA, 2017, pp. 1–5.

[6] *Rate of Change of Frequency (ROCOF) Withstand Capability, ENTSO-E Guidance Document for National Implementation for Network Codes on Grid Connection*, Eur. Netw. Transm. Syst. Oper. Electricity, Brussels, Belgium, Mar. 2017.

[7] L. Ruttledge, N. W. Miller, J. O'Sullivan, and D. Flynn, "Frequency response of power systems with variable speed wind turbines," *IEEE Trans. Sustain. Energy*, vol. 3, no. 4, pp. 683–691, Oct. 2012.

[8] V. Gevorgian, Y. Zhang, and E. Ela, "Investigating the impacts of wind generation participation in interconnection frequency response," *IEEE Trans. Sustain. Energy*, vol. 6, no. 3, pp. 1004–1012, Jul. 2015.

[9] *Inverter-Based Resource Performance Guideline*, Atlanta, GA, USA, North Amer. Elect. Rel. Corp., Sep. 2018.

[10] J. Johnson, J. C. Neely, J. J. Delhotal, and M. Lave, "Photovoltaic frequency–watt curve design for frequency regulation and fast contingency reserves," *IEEE J. Photovolt.*, vol. 6, no. 6, pp. 1611–1618, Nov. 2016.

[11] M. F. M. Arani and E. F. El-Saadany, "Implementing virtual inertia in DFIG-based wind power generation," *IEEE Trans. Power Syst.*, vol. 28, no. 2, pp. 1373–1384, May 2013.

[12] Z. Miao, L. Fan, D. Osborn, and S. Yuvarajan, "Wind farms with HVdc delivery in inertial response and primary frequency control," *IEEE Trans. Energy Convers.*, vol. 25, no. 4, pp. 1171–1178, Dec. 2010.

[13] J. Morren, S. W. H. de Haan, W. L. Kling, and J. A. Ferreira, "Wind turbines emulating inertia and supporting primary frequency control," *IEEE Trans. Power Syst.*, vol. 21, no. 1, pp. 433–434, Feb. 2006.

[14] Y. Zhang, A. Melin, S. M. Djouadi, M. M. Olama, and K. Tomsovic, "Provision for guaranteed inertial response in diesel-wind systems via model reference control," *IEEE Trans. Power Syst.*, vol. 33, no. 6, pp. 6557–6568, Nov. 2018.

[15] S. Laudahn, J. Seidel, B. Engel, T. Bülo, and D. Premm, "Substitution of synchronous generator based instantaneous frequency control utilizing inverter-coupled DER," in *Proc. IEEE 7th Int. Symp. Power Electron. Distrib. Gener. Syst. (PEDG)*, Vancouver, BC, Canada, 2016, pp. 1–8.

[16] M. Hadjikypris, V. Efthymiou, and G. E. Georghiou, "Enhanced frequency response of inverter dominated low inertia power systems," in *Proc. 1st Int. Conf. Energy Transition Mediterr. Area (SyNERGY MED)*, Cagliari, Italy, 2019, pp. 1–6.

[17] T. Xu, W. Jang, and T. Overbye, "Commitment of fast-responding storage devices to mimic inertia for the enhancement of primary frequency response," *IEEE Trans. Power Syst.*, vol. 33, no. 2, pp. 1219–1230, Mar. 2018.

[18] M. E. Elkhatib, W. Du, and R. H. Lasseter, "Evaluation of inverter-based grid frequency support using frequency-watt and grid-forming PV inverters," in *Proc. IEEE Power Energy Soc. Gen. Meeting (PESGM)*, Portland, OR, USA, 2018, pp. 1–5.

[19] Y. Zhang, M. E. Raoufat, K. Tomsovic, and S. M. Djouadi, "Set theory-based safety supervisory control for wind turbines to ensure adequate frequency response," *IEEE Trans. Power Syst.*, vol. 34, no. 1, pp. 680–692, Jan. 2019.

[20] A. Sangwongwanich, Y. Yang, and F. Blaabjerg, "A sensorless power reserve control strategy for two-stage grid-connected PV systems," *IEEE Trans. Power Electron.*, vol. 32, no. 11, pp. 8559–8569, Nov. 2017.

[21] S. You *et al.*, "Comparative assessment of tactics to improve primary frequency response without curtailing solar output in high photovoltaic interconnection grids," *IEEE Trans. Sustain. Energy*, vol. 10, no. 2, pp. 718–728, Apr. 2019.

[22] Y. Tan *et al.*, "Enhanced frequency regulation using multilevel energy storage in remote area power supply systems," *IEEE Trans. Power Syst.*, vol. 34, no. 1, pp. 163–170, Jan. 2019.

[23] M. Carrión, Y. Dvorkin, and H. Pandžić, "Primary frequency response in capacity expansion with energy storage," *IEEE Trans. Power Syst.*, vol. 33, no. 2, pp. 1824–1835, Mar. 2018.

[24] Y. Cui, Y. Liu, and Y. Liu, "Power system inertia estimation using synchrophasor frequency measurements," U.S. Patent 16 000 495, Dec. 2018.

[25] D. P. Chassin, Z. Huang, M. K. Donnelly, C. Hassler, E. Ramirez, and C. Ray, "Estimation of WECC system inertia using observed frequency transients," *IEEE Trans. Power Syst.*, vol. 20, no. 2, pp. 1190–1192, May 2005.

[26] P. M. Ashton, C. S. Saunders, G. A. Taylor, A. M. Carter, and M. E. Bradley, "Inertia estimation of the GB power system using synchrophasor measurements," *IEEE Trans. Power Syst.*, vol. 30, no. 2, pp. 701–709, Mar. 2015.

[27] F. Inoue, H. Taniguchi, Y. Ikeguchi, and K. Yoshida, "Estimation of power system inertia constant and capacity of spinning-reserve support generators using measured frequency transients," *IEEE Trans. Power Syst.*, vol. 12, no. 1, pp. 136–143, Feb. 1997.

[28] K. Tuttelberg, J. Kilter, D. Wilson, and K. Uhlen, "Estimation of power system inertia from ambient wide area measurements," *IEEE Trans. Power Syst.*, vol. 33, no. 6, pp. 7249–7257, Nov. 2018.

[29] M. Segal and Y. Xiao, "Multivariate random forests," *WIREs Data Min. Knowl. Discov.*, vol. 1, no. 1, pp. 80–87, 2011.

[30] J. Ma, Y. V. Makarov, R. Diao, P. V. Etingov, J. E. Dagle, and E. De Tuglie, "The characteristic ellipsoid methodology and its application in power systems," *IEEE Trans. Power Syst.*, vol. 27, no. 4, pp. 2206–2214, Nov. 2012.

[31] J. Ma, Y. V. Makarov, C. H. Miller, and T. B. Nguyen, "Use multi-dimensional ellipsoid to monitor dynamic behavior of power systems based on PMU measurement," in *Proc. IEEE Power Energy Soc. Gen. Meeting*, Pittsburgh, PA, USA, Jul. 2008, pp. 5151–5158.

[32] P. Kumar and E. A. Yildirim, "Minimum-enclosing ellipsoids and core sets," *J. Optim. Theory Appl.*, vol. 126, no. 1, pp. 1–21, Jul. 2005.

[33] W. Li, P. Du, and N. Lu, "Design of a new primary frequency control market for hosting frequency response reserve offers from both generators and loads," *IEEE Trans. Smart Grid*, vol. 9, no. 5, pp. 4883–4892, Sep. 2018.

[34] Y. Liu, S. You, J. Tan, Y. Zhang, and Y. Liu, "Frequency response assessment and enhancement of the U.S. power grids toward extra-high photovoltaic generation penetrations—An industry perspective," *IEEE Trans. Power Syst.*, vol. 33, no. 3, pp. 3438–3449, May 2018.

[35] Y. Liu *et al.*, "A distribution level wide area monitoring system for the electric power grid–FNET/GridEye," *IEEE Access*, vol. 5, pp. 2329–2338, 2017.

[36] K. Hornik, M. Stinchcombe, and H. White, "Multilayer feedforward networks are universal approximators," *Neural Netw.*, vol. 2, no. 5, pp. 359–366, Jan. 1989.

[37] R. Hecht-nielsen, "Theory of the backpropagation neural network," in *Proc. Int. Joint Conf. Neural Netw.*, vol. 1. Washington, DC, USA, Jun. 1989, pp. 593–611.

[38] *ERCOT Nodal Operating Guides, Section 2: System Operations and Control Requirements*," ERCOT, Austin, TX, USA, 2018.

[39] Y. Ma, J. Wang, F. Wang, and L. M. Tolbert, "Converter-based reconfigurable real-time electrical system emulation platform," *Chin. J. Elect. Eng.*, vol. 4, no. 1, pp. 20–27, Mar. 2018.

[40] Y. Cui, S. You, and Y. Liu, "Ambient synchrophasor measurement based system inertia estimation," in *Proc. IEEE Power Eng. Soc. Gen. Meeting*, 2020, pp. 1–5.

[41] L. Zhan *et al.*, "Fault-tolerant grid frequency measurement algorithm during transients," *IET Energy Syst. Integr.*, vol. 2, no. 3, pp. 173–178, Sep. 2020.